ELSEVIER

Soil Dynamics and Earthquake Engineering 23 (2003) 715–735

SOIL DYNAMICS AND EARTHQUAKE ENGINEERING

www.elsevier.com/locate/soildyn

Evaluation of hard rock spectral models for the Taiwan region on the basis of the 1999 Chi–Chi earthquake data

Vladimir Yu. Sokolov[a,*], Chin-Hsuing Loh[b,1], Kuo-Liang Wen[c,2]

[a]*Geophysical Institute of Karlsruhe University, Hertzstr. 16, 76187 Karlsruhe, Germany*
[b]*National Center for Research on Earthquake Engineering, 200, Sec. 3, Hsinhai Rd, Taipei, Taiwan, ROC*
[c]*Institute of Applied Geology, National Central University, Chung Li, Taoyuan county 32054, Taiwan, ROC*

Accepted 19 June 2003

Abstract

We analyze the ability of different spectral models to describe the frequency content of ground motion during the 1999 Chi–Chi earthquake ($M_W = 7.6$, Taiwan) and two large ($M_L = 6.8$) aftershocks. The spectral models evaluated include the one-corner model of Brune applied with various key parameters (seismic moment and stress drop), and the two-corner-frequency models proposed for eastern North America [Bull. Seismol. Soc. Am. 83 (1993) 1778] and California [Bull. Seismol. Soc. Am. 90 (2000) 255]. The ground-motion spectra predicted by these spectral models for hypothetical very hard rock site were compared with the Chi–Chi earthquake data obtained on rock (class B) and soft rock or very dense soil (class C) sites. The approach also allows us evaluating the generalized empirical amplification function for class B and C sites in the region.

It has been found that, the amplitude spectra of recorded ground acceleration (the mainshock and aftershocks) for frequencies larger than 0.3–0.4 Hz agree with the modelled two-corner-frequency spectra calculated using the model proposed for California. The single-corner-frequency model also provides a good agreement with the observations when using so-called 'short-period seismic moment' [Phys. Earth Planet. Interiors 37 (1985) 108] instead of the reported values obtained from long-period waves. The key parameters used in the single-corner model coincide with parameters of subsources evaluated for the complicated mainshock source. Therefore, it is possible to confirm the suggestion that the short-period seismic waves, at least for the thrust earthquakes, are generated mainly from the fracture of small-scale heterogeneities. The use of two-corner-frequency source model for earthquake spectrum that is based on long-period seismic moment value is equivalent, for frequencies larger than 0.3–0.4 Hz, to the use of single-corner-frequency model that is based on the parameters of major subsource.

© 2003 Elsevier Ltd. All rights reserved.

Keywords: Acceleration spectra; Amplification function; Chi–Chi earthquake

1. Introduction

Predicting and synthesizing strong ground motion expected during future earthquakes is one of the important problems of engineering seismology. The Fourier amplitude spectrum (FAS), among other parameters of earthquake ground motion, is widely used for estimating seismic hazard and strong ground-motion prediction. Peak amplitudes of ground acceleration and response spectra for various magnitudes, distances and site conditions may be estimated on the basis of stochastic simulation of ground-motion series [4,5] using FAS as input parameter [6–9]. On the other hand, FAS allows evaluation of seismic intensity in terms of MMI or MSK scales [10–12].

In one of the widely used approaches to describe the dependence of Fourier amplitude spectra on magnitude, distance and local soil condition the source, propagation, and site effects are considered separately by simple analytical expressions. The source spectra are often described by so-called single-corner-frequency Brune [13] model that represents seismic radiation from a point source. There are two key parameters in the model: seismic moment M_0, which is determined from long-period waves at teleseismic distances, and stress parameter $\Delta\sigma$, which characterizes the maximum velocity of slip on rupturing fault [14]. The applicability of the model has been tested for different seismic regions [5–7,15–19]. More complex, so-called two-corner-frequency models were proposed on the basis of

* Corresponding author. Fax: +49-721-71173.
E-mail addresses: vladimir.sokolov@gpi.uni-karlsruhe.de (V.Y. Sokolov); lohc@ncree.gov.tw (C.-H. Loh); wenkl@eqm.gep.ncu.edu.tw (K.-L. Wen).
[1] Fax: +886-2-2732-2223.
[2] Fax: +886-3-422-2044.

0267-7261/$ - see front matter © 2003 Elsevier Ltd. All rights reserved.
doi:10.1016/S0267-7261(03)00075-7

empirical data and theoretical proposition [1,20–23] to describe inhomogeneous faulting. It has been also shown [2] that the use of a two-corner point source model of the earthquake spectrum is equivalent to the use of a complex finite-fault model comprised of single-corner Brune subfaults. The lower corner is related to the size of the finite-fault, and the higher corner is related to the subfault size. The comparison of various spectral models in North America may be found, for example, in Ref. [2,24].

The region-dependent effects of propagation path are described by geometrical attenuation and dissipation of energy due to inelastic properties of the propagation medium. The models of source spectra and attenuation are evaluated on the basis of available ground-motion data and they are intended for description of general features of seismic excitation and propagation in a specific region. It is convenient to create the models for the case of hard rock or rock sites, and the site-specific estimations may be easily obtained using frequency-dependent amplification functions that reflect the response of the uppermost several hundred meters of rock and soil and the effect of surface topography. In certain cases (e.g. building codes provisions), it is sufficient to describe the variety of local soil conditions by a few number of generalized site classes. In recent years, the attempts were made for developing of frequency-dependent amplification functions, both for the case of response spectra [25] and Fourier amplitude spectra [26,27], that describe typical soil columns (site classes). The site classification system that is widely used at present [28,29] is based on the properties of top 30 m of soil column, disregarding the characteristics of the deeper geology. Six site categories are defined on the basis of averaged shear waves velocity, namely: A, hard rock; B, rock; C, very dense or stiff soil; D, stiff soil; E, soft soil; F, soils requiring special studies (Table 1).

In this context, the specifications of 'hard rock' spectrum for future earthquake is of particular significance for ground-motion predictions. It has been shown [2] on the basis of Californian earthquakes with magnitudes 4.5–7.5 and distances from 0 to 200 km that stochastic finite-fault simulations or equivalent two-corner point source may be considered as a robust and accurate approach to estimate ground motions. However, the relation between key parameters of the two-corner-frequency spectral models (seismic moment and corner frequencies) seems to be region-dependent [24]. Therefore, a special study should be performed to evaluate the ability of existing spectral models to predict features of seismic radiation from large and possibly complicated future earthquakes in a given region. By the other words, it is necessary to obtain answers on the following question. What type of modelling (Green functions, combined Green functions-stochastic, finite-fault stochastic, equivalent two-corner point source, etc.) may be used, bearing in mind the sensitivity of ground motions to the specific aspects of the source and propagation path? What key parameters should be accepted for the given type of modelling? What are the most important parameters which should be used for strong ground-motion simulation for the purposes of seismic hazard assessment?

Table 1
Comparison between the 1997 UBC Provisions and the Simplified Site Classification Working Scheme used in Taiwan [37]

Site class	Site class description of 1997 UBC Provisions	Site class description of Simplified Working Scheme [37]
A	Hard rock, eastern United States only, $V_s > 1500$ (m/s)	Not used
B	Rock, V_s is 760–1500 m/s	Miocene and older strata, limestone, igneous rocks, and metamorphic rocks
C	Very dense soil and soft rock, V_s is 360–760 m/s.	Pliocene and Pleistocene strata, conglomerates, pyroclastic rocks, etc. and geomorphologic lateric terraces
D	Stiff soils V_s is 180–360 m/s.	Late Pleistocene and Holocene strata, geomorphologic fluvial terrace
E	Soft soils, profile with more than 10 ft (3 m) of soft clay	Holocene deposits and fills
F	Soils requiring site specific evaluations: 1. Soil vulnerable to potential failure or collapse under seismic loading 2. Peats and/or highly organic clays 3. Very high plasticity clays 4. Very thick soft/medium stiff clays	Not classified in Ref. [37]

The empirical databases that are used for evaluation of spectral models usually consist on the recording which were obtained during the events of small and moderate magnitudes. The lack of data of large earthquakes makes the problem of reliable ground-motion prediction questionable. On the one hand, sometimes it is possible to modify the well-based ground-motion relations, for example Californian data, for use in the cases of limited databases, such as eastern North America [24,30]. On the other hand, every strong earthquake provides a unique opportunity both to verify the accepted attenuation models, and to update empirical relationships. The most impressive example of such informative events is the recent Chi–Chi (Taiwan) $M_W = 7.6$ earthquake which produced a rich set of strong ground-motion recordings [31–33]. The models for Fourier acceleration spectra of ground acceleration in the Taiwan region have been proposed before the Chi–Chi earthquake on the basis of the recordings (1380 accelerograms) of small and moderate earthquakes ($4.5 < M_L < 6.5$) [34,35]. The applicability of 'average soil' spectral model for the case of the Chi–Chi earthquake data was tested in our previous article [36]. It has been shown that, in general, the local magnitude-based 'average soil' spectral model, which was recently developed for the Taiwan region, may be applied for prediction of spectral amplitudes within frequency range

0.3–12 Hz and peak ground acceleration (PGA) for larger reverse-fault earthquakes, even for epicentral area (source-to-site distances less than 15–20 km).

The goal of this article is to analyze the ability of various 'hard rock' spectral models, including the model proposed for the Taiwan region, to describe the frequency content of ground motions during the Chi–Chi earthquake consequence (the mainshock and two strong aftershocks). On the one hand, the study allows us to test applicability of various spectral models in the case of shallow large and complicated earthquakes in Taiwan. On the other hand, the generalized empirical amplification function has been evaluated for rock (class B) and soft rock or very dense soil (class C) sites in the region.

2. The Chi–Chi earthquake data

The Chi–Chi, Taiwan earthquake of September 21, 1999, and aftershocks produced a rich set of strong ground-motion recordings [31–33] registered by the Taiwan Strong-motion Instrumentation Program (TSMIP) stations. The free-field strong-motion station sites were recently classified [37] using a scheme compatible with the 1994 and 1997 NEHRP provisions [29]. The existing geological and geomorphologic data were analyzed and the response spectral shape and the horizontal-to-vertical spectral ratio data were used. The site classification is as follows: B (rock); C (soft rock or very dense soil), D (stiff soil). Site class A (hard rock) is not applicable in Taiwan due to the wet climate and extremely high weathering. Site classes B and C can be distinguished by their geological age and rock type. Site class B may include igneous and metamorphic rocks, limestone and hard volcanic deposits. Sandstones, shales, conglomerates of Miocene age or older are all classified as class B. Most class B sites are located at hilly and mountainous highlands, except for some on limestone, igneous and metamorphic rock sites at lower elevations. Pliocene and Pleistocene sandstones, shale/mudstones, and conglomerates, volcanic breccias and pyroclastic rock of a similar age are classified as class C. Most class C sites are to be found on lateric terraces and highlands. Fig. 1 shows location of free-field TSMIP stations with emphasis on those classified as site class B and C.

When the research was being carried out, the data from four events of the Chi–Chi earthquakes sequence (the mainshock and three aftershocks) were processed and compiled in a form suitable for computer [32]. In this study, we used acceleration records which were obtained during the Chi–Chi mainshock ($M_L = 7.3$, $M_W = 7.6$) and two largest aftershocks ($M_L = 6.8$). The parameters of the events are listed in Table 2, and the epicenters are shown in Fig. 1. The information on class B and C stations recorded the earthquakes is listed in Tables 3 and 4. Fig. 2 show distribution of maximum recorded acceleration values (horizontal components) with emphasis on class B and

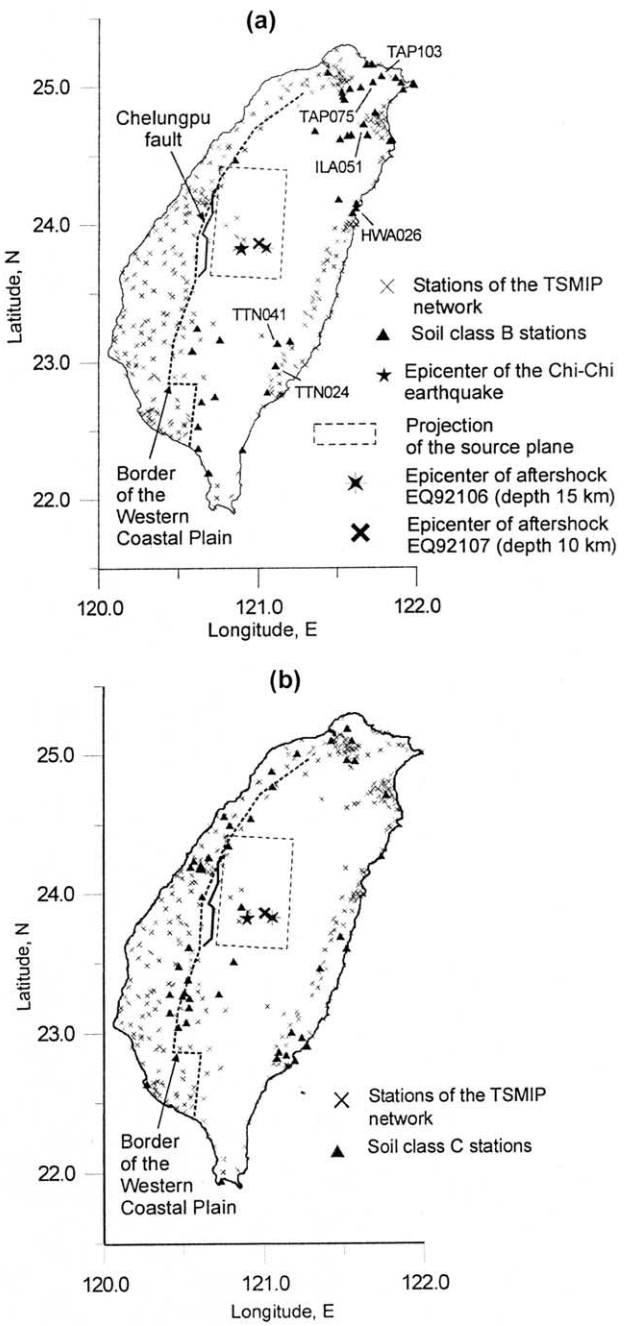

Fig. 1. Epicenters of the earthquakes (mainshock and two aftershocks), recordings of which were used in this study, and location of the free-field digital accelerograph stations (TSMIP network). Stations of assigned site (a) class B and (b) class C are distinguished.

class C stations versus distance for the considered earthquakes. The shortest distance between the source plane (surface of fault slippage) and the station is used for the mainshock. The model of the mainshock source proposed in Ref. [38] (see also http://wwweic.eri.utokyo.ac.jp/yuji/taiwan/taiwan.html) is shown in Fig. 1 (strike, 3°; dipping angle, 29° to the East; length of the source, 90 km and width, 45 km). There is no information on the aftershock source models and the hypocentral distance are used for the cases.

Table 2
Parameters of the Chi–Chi earthquake mainshock and aftershocks, recordings of which are used in this study

Earthquake code	Date and time (UT)	Latitude (N)	Longitude (E)	Depth (km)	M_L	Moment[a] (dyn cm)	Moment magnitude[a]
EQ92101 (mainshock)	1999/09/20 17:47:15	23°51.15′	120°48.93′	8.0	7.3	3.38×10^{27}	7.6
EQ92106	1999/09/22 00:14:40	23°49.58′	121°02.80′	15.6	6.8	5.03×10^{25}	6.4
EQ92107	1999/09/25 23:52:49	23°51.56′	121°00.35′	10	6.8	6.01×10^{25}	6.5

[a] Harvard CMT Catalog (www.seismology.harvard.edu).

The analyses of the peak ground motions showed [39–41] that the Chi–Chi earthquake dataset is characterized by the certain peculiarities. When considering the distribution of ground-motion amplitudes versus closest distance to the surface rupture (Chelungpu fault), the overall level of the observed horizontal PGAs from the earthquake are about 50% below the median PGA based on commonly used attenuation in California for $M_W = 7.6–7.7$ [42–44]. The Chi–Chi PGA values are equivalent to what would be predicted for $M_W = 6.6$, 6.0, and 6.2 from Campbell's, Boore et al.'s and Sadigh et al.'s attenuation models, respectively [40]. Unlike the horizontal PGA, the peak ground velocity (PGV) values are relatively high (about 80% higher) than those predicted by existing PGV attenuation model [43]. Therefore, the Chi–Chi

Table 3
Parameters of site class B stations and availability of records (source-to-site distances in km) obtained during the analyzed earthquakes

Station code	Longitude	Latitude	Elevation (m)	Mainshock	EQ92106	EQ92107
CHY102	120.614	23.246	557	45	47	50
HWA023	121.596	24.080	44	72	–	70
HWA026	121.617	24.119	32	76	80	75
HWA046	121.621	24.149	49	–	85	75
HWA056	121.508	24.180	440	70	80	70
ILA019	121.693	24.644	114	–	–	115
ILA024	121.588	24.645	211	90	110	115
ILA025	121.566	24.640	271	–	–	110
ILA031	121.834	24.600	20	100	120	–
ILA051	121.667	24.721	119	95	115	120
ILA052	121.849	24.609	32	105	115	120
ILA054	121.918	24.973	38	125	150	160
ILA057	121.741	24.807	51	–	–	135
ILA063	121.518	24.616	300	80	90	105
KAU034	120.620	22.529	105	–	125	–
KAU038	120.685	22.192	15	–	150	–
KAU047	120.583	23.082	292	68	68	70
KAU050	120.757	23.163	635	57	55	60
KAU051	120.620	22.372	74	–	140	–
KAU077	120.723	22.747	830	–	95	100
KAU078	120.641	22.711	148	–	105	115
TAP034	121.530	24.955	41	105	135	–
TAP035	121.535	24.923	46	105	130	130
TAP036	121.545	24.904	73	105	128	–
TAP059	121.686	25.157	90	135	170	160
TAP060	121.724	25.157	31	135	175	–
TAP067	121.580	24.980	220	115	155	145
TAP069	121.988	25.008	110	145	160	–
TAP072	121.650	24.991	160	120	140	–
TAP075	121.728	25.029	228	125	145	155
TAP078	121.872	25.056	65	140	155	–
TAP079	121.906	25.024	24	140	150	–
TAP081	121.981	25.018	4	147	160	–
TAP103	121.781	25.071	380	135	155	160
TAP104	121.720	25.158	63	–	155	165
TCU046	121.854	24.468	224	36	70	70
TCU085	121.358	24.676	660	–	110	100
TTN024	121.108	22.973	275	85	95	85
TTN028	121.054	22.779	138	–	100	90
TTN040	121.198	23.157	284	75	65	70
TTN041	121.118	23.134	440	73	68	70

Table 4
Parameters of site class C stations and availability of records (source-to-site distances in km) obtained during the analyzed earthquakes

Station code	Latitude	Longitude	Elevation (m)	Mainshock	EQ92106	EQ92107
CHY022	23.046	120.462	100	–	70	61
CHY029	23.6143	120.5288	107	25	35	20
CHY046	23.4768	120.4632	67	30	25	25
CHY050	23.281	120.4083	38	50	55	43
CHY052	23.2882	120.501	470	45	50	36
CHY057	23.149	120.41	62	–	65	55
CHY061	23.077	120.511	114	–	67	57
CHY074	23.5103	120.8052	2400	25	–	–
CHY079	23.1848	120.528	234	50	50	45
CHY081	23.2665	120.488	476	45	53	40
CHY087	23.3837	120.522	165	30	35	29
CHY0109	23.2517	120.5295	220	45	52	–
HWA002	23.601	121.512	5	–	53	55
HWA022	24.2675	121.7325	10	70	54	65
HWA033	23.6863	121.474	110	45	47	50
HWA038	23.4605	121.3442	230	45	42	52
ILA010	24.7088	121.7628	45	90	105	110
KAU054	23.278	120.713	720	–	40	30
KAU057	22.6343	120.2635	130	110	–	–
TAP066	25.1865	121.5202	820	110	145	–
TAP086	24.9522	121.5673	128	90	125	130
TAP087	25.1008	121.4177	134	100	134	140
TAP098	25.0997	121.5487	140	100	137	144
TCU008	25.0093	121.2062	84	80	120	125
TCU018	24.8803	121.045	112	65	105	110
TCU029	24.5588	120.749	37	–	65	81
TCU039	24.4922	120.7838	158	20	49	75
TCU045	24.541	120.914	210	–	64	69
TCU048	24.1807	120.5928	163	20	–	–
TCU057	24.178	120.6105	86	20	35	–
TCU070	24.196	120.54	10	–	41	–
TCU087	24.348	120.773	258	–	44	60
TCU089	23.9037	120.8565	700	15	–	–
TCU094	24.7693	121.0485	128	50	91	100
TCU100	24.186	120.6152	95	20	–	49
TCU104	24.2097	120.6017	207	25	44	50
TCU105	24.2387	120.5595	20	30	45	55
TCU120	23.98	120.613	230	–	–	32
TCU136	24.26	120.652	170	–	41	55
TTN018	22.8207	121.0717	170	90	85	–
TTN025	22.9037	121.263	275	80	80	75
TTN026	22.863	121.083	230	–	82	77
TTN044	23.007	121.165	200	–	70	–
TTN046	22.966	121.232	180	–	68	75
TTN047	22.84	121.131	112	–	82	85

earthquake was called as HV-LA (high-PGV, low-PGA) earthquake. It is necessary to note that the most part of the stations to the West and South from the epicenter are located in deep alluvium plain area (the Western Coastal plain, WCP; see Fig. 1). The long-period waveforms that include significant surface waves appears to be the common ground-motion characteristics in the area [45,46].

3. Description of spectral models

The general model for the Fourier acceleration spectrum A at frequency f is given by

$$A(f) = (2\pi f)^2 CS(f)D(R,f)I(f) \quad (1)$$

where C is the scaling factors; $S(f)$ is the source spectrum; $D(R,f)$ is the attenuation function, and $I(f)$ represents frequency-dependent site response. The scaling factor is calculated as

$$C = (\langle R_{\theta\phi}\rangle FV)/(4\pi\rho\beta^3 R^b) \quad (2)$$

where $\langle R_{\theta\phi}\rangle$ is the radiation coefficient, F is the free surface amplification, V represents the partitions of the vector into horizontal components, ρ and β are the density and shear velocity in the source region, and R is the source–site distance. A commonly used source function $S(f)$ in the Brune [13] single-corner-frequency model is

$$S(f) = M_0/[1 + (f/f_0)^2] \quad (3)$$

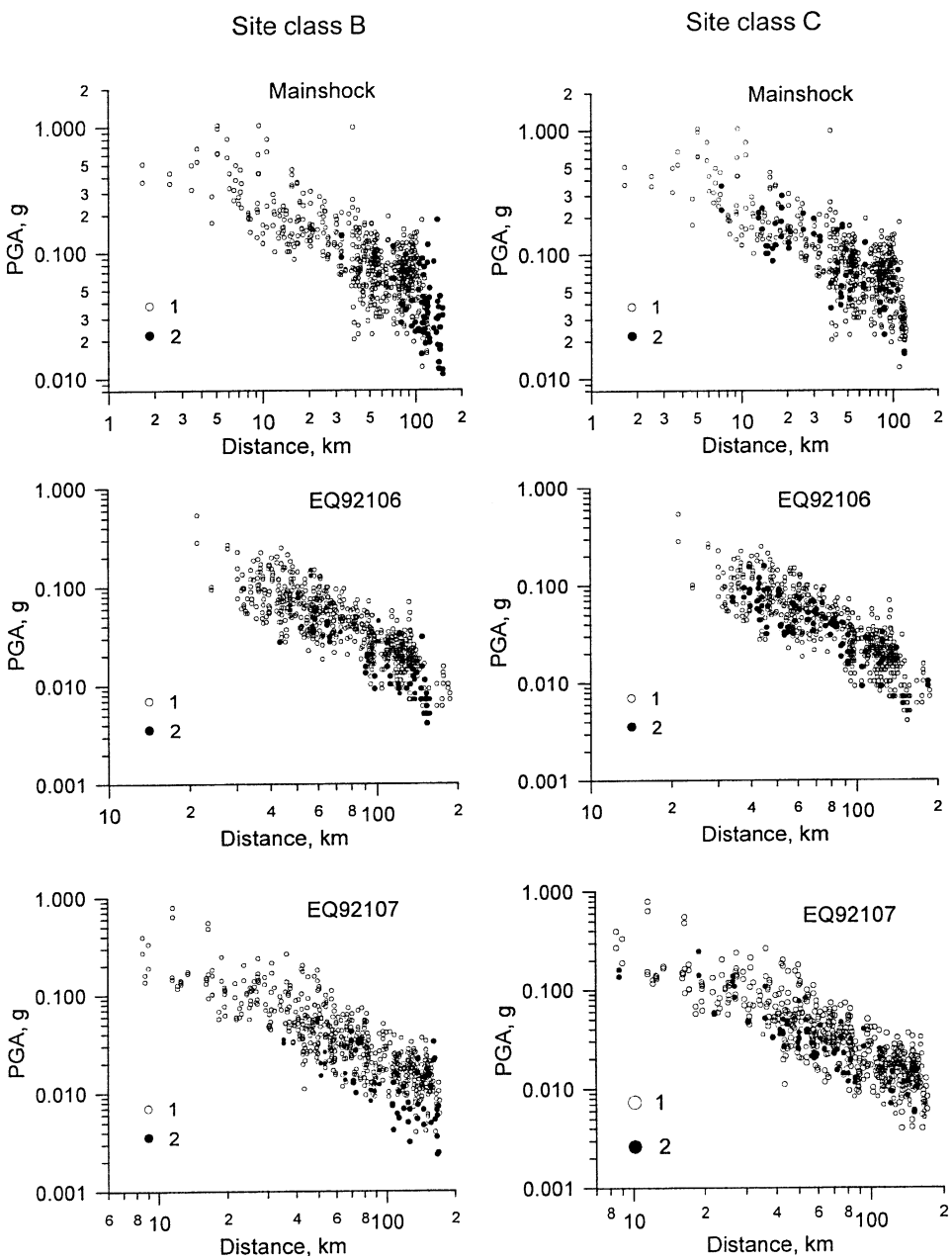

Fig. 2. Distribution of horizontal peak ground acceleration (PGA) values versus distance for the Chi–Chi earthquake mainshock and considered aftershocks. (1) Empty circles denote PGAs regardless of the site classes, (2) black circles show PGAs for selected (B or C) site classes.

For the model, the source acceleration spectrum at low frequencies increases as f^2 and approaches a value determined by f_0 (corner-frequency) and M_0 at frequencies $f > f_0$. The value of f_0 can be found from the relation $f_0 = 4.9 \times 10^6 \beta(\Delta\sigma/M_0)^{1/3}$. Here $\Delta\sigma$ is the stress parameter in bars, M_0 is the seismic moment in dyn cm and β in km/s. The following functional form for two-corner-frequency spectrum was suggested by Atkinson [1]

$$S(f) = M_0\{(1-\varepsilon)/[1+(f/f_a)^2] + \varepsilon/[1+(f/f_b)^2]\} \quad (4)$$

where f_a and f_b are the lower and higher corner frequencies; ε is the weighting parameter. For eastern North America, the parameters for moment magnitudes $M > 5$ were obtained as follows

$$\begin{aligned} \log f_a &= 2.41 - 0.533M \\ \log f_b &= 1.43 - 0.188M \\ \log \varepsilon &= 2.52 - 0.637M \end{aligned} \quad (5)$$

and for California [2]

$$\begin{aligned} \log f_a &= 2.181 - 0.496M \\ \log f_b &= 2.41 - 0.408M \\ \log \varepsilon &= 0.605 - 0.255M \end{aligned} \quad (6)$$

These models are further mentioned as ENA- and CAL-models, respectively.

For the Taiwan region (TWN-model) it has been proposed [34,35] to use the single-corner-frequency Brune source model (Eqs. (1)–(3)) for hypothetical *very hard rock* (VHR) sites ($\rho = 2.8$ gm/cm^3, $\beta = 3.8$ km/s, $I(f) = 1$). High-frequency amplitudes are reduced, through the kappa operator [47], by multiplying the spectrum by the factor $\exp(-\pi\kappa f)$ ($\kappa = 0.03$). The seismic moment M_0 and stress parameter $\Delta\sigma$ are determined using recently proposed regional relationships between M_0 and magnitude (M_L) [48]

$$\log M_0 = (19.043 \pm 0.533) + (0.914 \pm 0.035)M_L \quad (7)$$

and between $\Delta\sigma$ and M_0 [49]

$$\log \Delta\sigma = -3.3976 + 0.2292 \log M_0 (\pm 0.6177) \quad (8)$$

Tsai also noted that the $\Delta\sigma$ values estimated using his relationships should be treated as upper-boundary values.

The function $D(R,f)$ accounts for frequency-dependent attenuation that modifies the spectral shape in the following form

$$D(R,f) = \exp[-\pi f R/Q(f)\beta] \quad (9)$$

Frequency-dependent inelastic attenuation of spectral amplitudes with distance for the Taiwan region may be described using quality factor $Q = 225f^{1.1}$ for deep (depth more than 35 km) earthquakes and $Q = 125f^{0.8}$ for shallow earthquakes. When considering geometrical spreading in the form $1/R^b$ (Eq. (2)), attenuation of the direct waves is described using $b = 1.0$ for $R_1 < 50$ km; for transition zone where the direct wave is joined by postcritical reflections from mid-crustal interfaces and the Moho-discontinuity ($50 < R_2 < 150$–170 km) $b = 0.0$, and attenuation of multiply reflected and refracted S-waves is described by $b = 0.5$ for $R_3 > 170$ km.

The VHR model was used for determination of local site response characteristics for the territory of Taipei city [50] in terms of frequency-dependent amplification (spectral ratios). The approach consisted in calculating spectral ratios between spectra of actual earthquake records (horizontal components) and those modelled for a VHR site [51]. The spectral model along with the corresponding site amplification characteristics was used for evaluation of site and region-dependent ground-motion parameters [52] and probabilistic seismic hazard assessment [53] for the Taipei area. These spectral ratios reflect the difference between idealized source scaling and attenuation models and real recordings. Besides local site response, the ratios between observed and modelled spectra include effects of source rupture peculiarities and inhomogeneous propagation path. However, when using a large enough number of records from earthquakes varied by magnitude, source depth and azimuth, the effects of focal mechanism and directivity are expected to be averaged out. It has been shown that empirical ratios between the observed and modelled spectra reveal a good agreement with theoretical spectral amplification of multilayered soil columns that was based on available geological and geotechnical information.

Thus, in the considered case of three earthquakes and more than 30 stations located at different distances (20–150 km) and directions from the source for every soil class we suppose that the results may be considered as generalized site effect.

4. Comparison of empirical and modelled data

4.1. The technique

The applicability of 'hard rock' spectral models may be tested by comparison of spectra of real recordings and modelled spectra. The modelled spectra should match the averaged observed 'hard rock' spectra. However, there are no sites in Taiwan to be classified as hard rock (class A) sites [37] and we use the following procedure in our study. As it follows from results obtained in Refs. [26,27], the amplitude of amplification functions for generalized site classes increases with frequency from unity up to a maximum value that, together with the frequency of the maximum, depends on the soil class and regional crustal properties. The amplitudes decrease rapidly for the higher frequencies. The amplification for site class B (rock) is characterized by the lowest maximum amplitude (1.4–1.5) and the highest frequency of the maximum (3–4 Hz) [26]. Thus, when comparing with the class B observed spectra, the modelled hard rock spectra should fit the empirical ones at low frequencies. The intermediate frequency amplitudes of hard rock spectra should be less than the observed ones at frequencies up to 7–10 Hz. Ideally, for the case of linear soil response on earthquake motion, the site amplification functions or ratio between observed and modelled spectra should not depend on magnitude. On the other hand, site effect should be independent of the source model applied. Therefore, if the proper spectral models are used for various magnitudes, the characteristics (averaged amplitudes and shape) of ratios between observed and modelled spectra should be approximately the same for different earthquakes (small and large, homogeneous and complicated), at least for those of similar distance and azimuth.

When constructing the modelled spectra for the considered earthquakes, we use the following key parameters (seismic moment M_0 and stress parameter $\Delta\sigma$). First, the value of seismic moment M_0 reported for the event in the Harvard CMT Catalogue was used for the single-corner-frequency model and empirical two-corner-frequency models (ENA and CAL). Two values of the stress parameter, namely 20 and 150 bars, were used for the single-corner-frequency model.

Second, we used one-corner-frequency TWN-model based on the regional relationships between M_0 and local magnitude M_L (Eq. (7)). Strictly speaking, the seismic moment that is associated with the local magnitude, should

Table 5
Parameters of the Chi–Chi earthquake mainshock and considered aftershocks that were reported and used for modelling

Event	Seismic moment, M_0 (dyn cm)[a]	Moment magnitude, M_W[a]	Local magnitude, M_L	Seismic moment (dyn cm) evaluated from Eq. (7) (mean value and confidence limits)	Seismic moment (dyn cm) used in asperity-based calculations	'Short-period seismic moment', M_1 (dyn cm)	Stress parameter (bars) evaluated from Eq. (8) and used for calculation (asperity-based)
Mainshock	$0.5–3.3 \times 10^{27}$	7.2–7.7	7.3	5.2×10^{25} ($0.0825–3.2 \times 10^{26}$)	1.0×10^{26}	$0.8–1.6 \times 10^{26}$	315 (200)
EQ92106	5.0×10^{25}	6.4	6.8	1.8×10^{25} ($0.3–10.7 \times 10^{25}$)	1.0×10^{25}	$1.0–2.0 \times 10^{25}$	250 (150)
EQ92107	6.0×10^{25}	6.5	6.8	1.8×10^{25} ($0.3–10.7 \times 10^{25}$)	1.4×10^{25}	$1.0–2.0 \times 10^{25}$	250 (150)

[a] The values for the mainshock are taken from different published sources.

be called as a 'sho=rt-period seismic moment', or M_1 following Koyama and Zheng [3] and Koyama [54], because the local magnitude is determined using Wood–Anderson seismograph with dominant period of 0.8 s. The maximum value of stress parameter for this case was evaluated using Eq. (8).

It is necessary to bear in mind confidence limits of the values of seismic moment and stress parameter, as far as the limited amount of the data used when obtaining the relationships (7) and (8). Thus, to reduce the number of possible values of key parameters within the confidence limits, we also use the values suggested by Irikura et al. [55] for the asperities of the Chi–Chi mainshock fault model. The single-corner-frequency TWN-model, which is based on these parameters, provided the third type of the modelled spectra. The choice of the parameter values is discussed in every case below. Table 5 summarizes the values of seismic moment and stress parameter used for the modelling.

4.2. The Chi–Chi earthquake aftershocks, event EQ92106, site class B

The value of seismic moment M_0 reported for the event in the Harvard CMT Catalogue is 5.03×10^{25} dyn cm that corresponds to moment magnitude M_W 6.4. First, the spectra were modelled for the M_0 value using Eqs. (1)–(3) and (9) for the case of single-corner-frequency spectral model and Eqs. (1), (2), (4)–(6) and (9) for the case of empirical two-corner-frequency models, which were proposed for eastern North America and California. Second, the single-corner-frequency spectra were modelled using the mean value of M_1 determined by Eq. (7) for local magnitude 6.8 (reported by CWB, Table 2) namely: 1.8×10^{25} dyn cm (confidence limits between 3.0×10^{24} and 1.07×10^{26} dyn cm). The mean value of seismic moment is close to 'short-period seismic moment' value ($1.0–2.0 \times 10^{25}$ dyn cm) that can be evaluated from 'seismic moment–short-period seismic moment' relationship suggested in Refs. [3,45] (see Figs. 2–12 in Ref. [45]). The value of stress parameter was accepted as 250 bars (Eq. (8)). Third, we also use the values suggested in Ref. [55] for one of the small asperities of the Chi–Chi mainshock fault model, namely: seismic moment of 1.0×10^{25} dyn cm and stress parameter of 150 bars. The choice was based on assumption that aftershocks may be considered to be delayed subsources [20]. For this earthquake, frequency-dependent attenuation of spectral amplitudes with distance for all spectral models is described using equality factor $Q = 125f^{0.8}$ [36].

Fig. 3 shows comparison between spectra of horizontal components of the record obtained at stations ILA051 and HWA026 and theoretical rock-site spectra. The stations were chosen as typical examples and location of the stations is shown in Fig. 1a. On the one hand, it is not possible to use the single-corner spectra based on the reported Harvard seismic moment value (Fig. 3b) for description of hard rock spectra. The two-corner-frequency models exhibit a better agreement with the observed spectra at low frequencies (Fig. 3b). On the other hand, the single-corner-frequency TWN-spectra based on parameters of the Chi–Chi mainshock asperity in general provides the best fit for the low-frequency parts of empirical and modelled spectra (Fig. 3c). Therefore, for evaluation of soil-B amplification functions, we used three models of hard rock spectra, namely: both (ENA and CAL) two-corner-frequency models (seismic moment of 5.03×10^{25} dyn cm) and single-corner-frequency model (seismic moment of 1.0×10^{25} dyn cm and stress parameter of 150 bars). Fig. 4 shows comparison of characteristics of the frequency-dependent amplification evaluated as the ratio between observed spectra (horizontal components) and corresponding modelled spectra. Surprisingly, the two-corner Californian model and single-corner TWN-model give almost the same amplification for frequencies greater than 0.4 Hz.

4.3. The Chi–Chi earthquake aftershocks, event EQ92107, site class B

The value of seismic moment M_0 reported for the event in the Harvard CMT Catalogue is 6.01×10^{25} dyn cm that corresponds to moment magnitude M_W of 6.5. Therefore, the single-corner and two-corner-frequency spectra were modelled using the value. As that for the case of event EQ92106, we also modelled single-corner-frequency spectra for two pair of the key parameters, namely: $M_0 = 1.8 \times 10^{25}$ dyn cm and stress parameter $\Delta\sigma = 250$ bars, which are based on Eqs. (7) and (8) for $M_L = 6.8$; $M_1 = 1.0 \times 10^{25}$ dyn cm and $\Delta\sigma = 150$ bars, which are based on parameters of

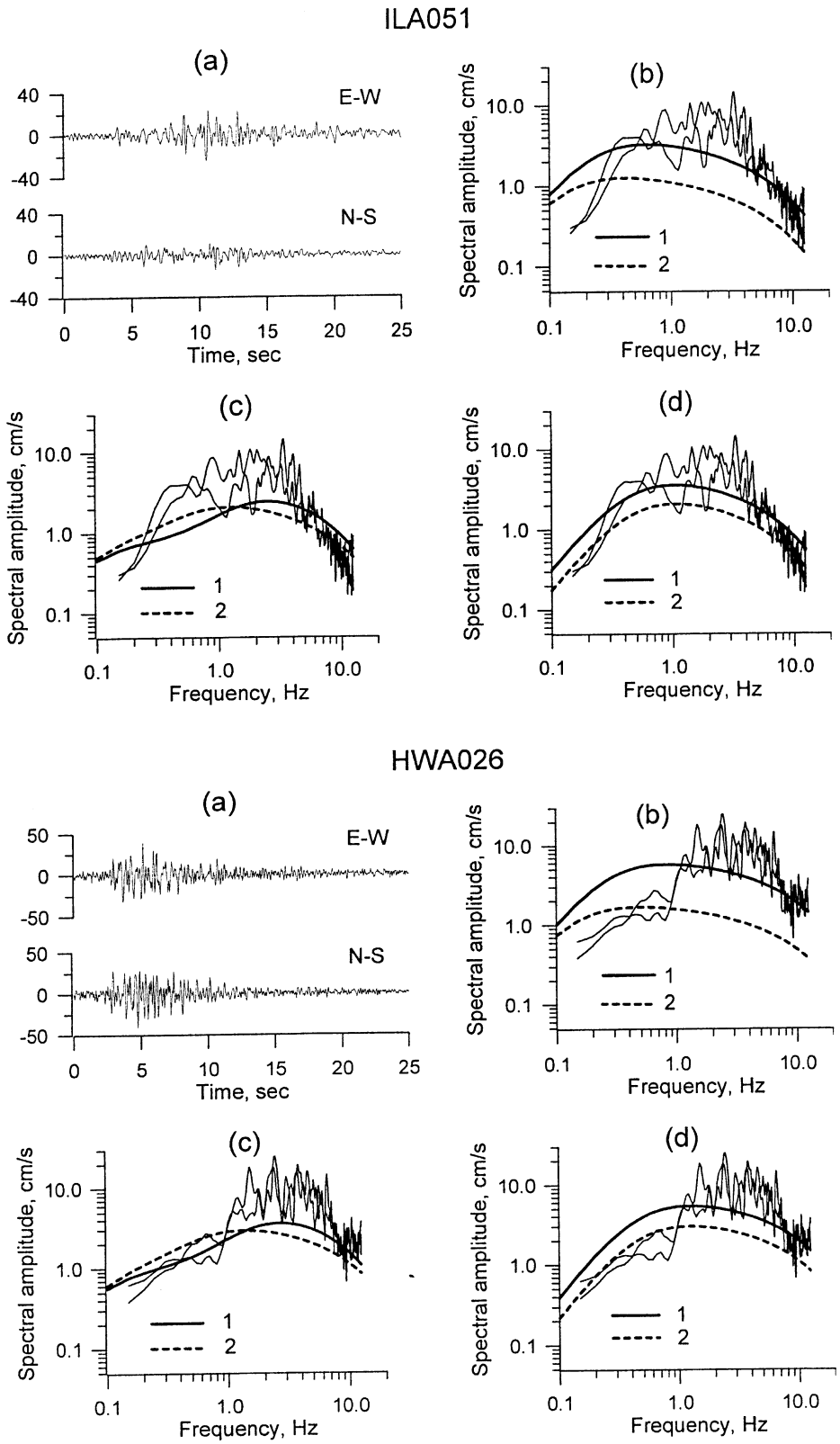

Fig. 3. Aftershock EQ92106, examples of comparison between observed and modelled data. a, Horizontal components of ground acceleration recordings, cm/s^2; b,c,d, comparison between observed Fourier amplitude spectra of ground acceleration (horizontal components, thin lines) and simulated very hard rock spectra (thick lines); b, single-corner-frequency model, $M_0 = 5.0 \times 10^{25}$ dyn cm, $\Delta\sigma = 150$ bars (line 1) and 20 bars (line 2); c, two-corner-frequency models, $M_0 = 5.0 \times 10^{25}$ dyn cm, ENA-model (line 1) and CAL-model (line 2); d, single-corner-frequency model, $M_0 = 1.8 \times 10^{25}$ dyn cm, $\Delta\sigma = 250$ bars (line 1) and $M_0 = 1.0 \times 10^{25}$ dyn cm, $\Delta\sigma = 150$ bars (line 2).

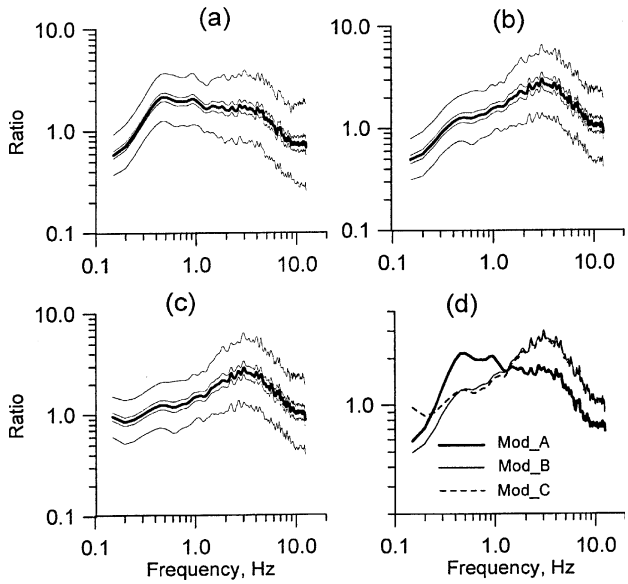

Fig. 4. Aftershock EQ92106. Characteristics of site class B amplification functions (ratio between observed and modelled spectra); thick lines show mean-amplitude values, thin lines denoted ± 1 standard deviation of the mean (standard error) and ± 1 standard deviation limits. a, Two-corner-frequency ENA-model of the very hard rock spectra; b, two-corner-frequency CAL-model; c, single-corner-frequency model ($M_0 = 1.0 \times 10^{25}$ dyn cm, $\Delta\sigma = 150$ bars); d, comparison of the mean-amplitude amplification functions evaluated using the considered (plots a, b, c) models.

the mainshock small asperity. For this shallow event (hypocentral depth 10 km), frequency-dependent attenuation of spectral amplitudes with distance is described using quality factor $Q = 80f^{0.8}$ [36]. Fig. 5 shows comparison between observed acceleration spectra fro soil class B stations ILA051 and TTN041 (see Fig. 1a) and theoretical spectra. When using the Harvard seismic moment value, the two-corner-frequency models show a better agreement with the observed spectra at low frequencies (Fig. 5c) than the single-corner-frequency model (Fig. 5b). On the one hand, the single-corner spectra based on the parameters determined from Eqs. (7) and (8) in general provides the best fit for the low-frequency parts of empirical and modelled spectra than the spectra based on the asperity parameters (Fig. 5c). Thus, to be consistent in the choice of key parameters and bearing in mind that reported value of seismic moment for event EQ92107 is higher than that for event EQ92106 (Table 2), for evaluation of site-B amplification function we used the following parameters of single-corner-frequency spectral model, namely: seismic moment of 1.4×10^{25} dyn cm and stress parameter of 150 bars.

Fig. 6 shows comparison of the characteristics of frequency-dependent amplification evaluated using these models. The mean-amplitude amplification curves obtained for the case of event EQ92106 are also shown in the figure. In general, the amplification functions calculated using the same hard rock model for these two aftershocks reveal the similar shapes and amplitudes. However, in the case of EQ92107 event, there is an additional amplification at frequencies 0.7–1.0 Hz as compared with that for EQ92106 event. The same phenomenon was observed when we compared recorded spectra with 'average soil' model [36]. The averaged ratio between observed and modelled 'average soil' spectra for aftershock EQ92106 (depth 15 km) exhibit amplitudes that are close to unity for the whole considered frequency range (0.2–12 Hz). The average ratio for aftershock EQ92107 (depth 10 km) shows amplification for frequencies 0.3–1.0 Hz. It was suggested that the narrow-band amplification reflects the influence of relatively long-period waves during shallow earthquakes of magnitudes 6.5–7.0, or so-called 'shallow earthquake effect'.

4.4. The Chi–Chi earthquake mainshock, site class B

The ground-motion data from the large and complex Chi–Chi earthquake are characterized by several peculiarities, which may be described by a joint influence of the effects of rupture propagation along the fault plane, shallow crustal structure and subsurface geological condition [40,45,46,56–58]. These peculiarities include the anomalous movement of sediments along the Chelungpu fault due to impact from deep faulting, the long-period waveforms including significant surface waves in deep alluvium plane area (WCP), the ground motion enhancing to the North from the source at the epicentral distances between 80 and 120 km at frequency range less than 1 Hz, and the deep basin response. However, it has been shown [36] that in the cases when the ground motions are not affected by these phenomena (epicentral zone, eastern and southern direction from the source at distances up to 80–90 km), the modelled 'average soil' spectra exhibit a good agreement with the observed spectra at frequencies greater than 0.2 Hz. Therefore, at the beginning, we consider the recordings obtained at soil class B stations located toward eastern and southern directions from the mainshock source (see Fig. 1a).

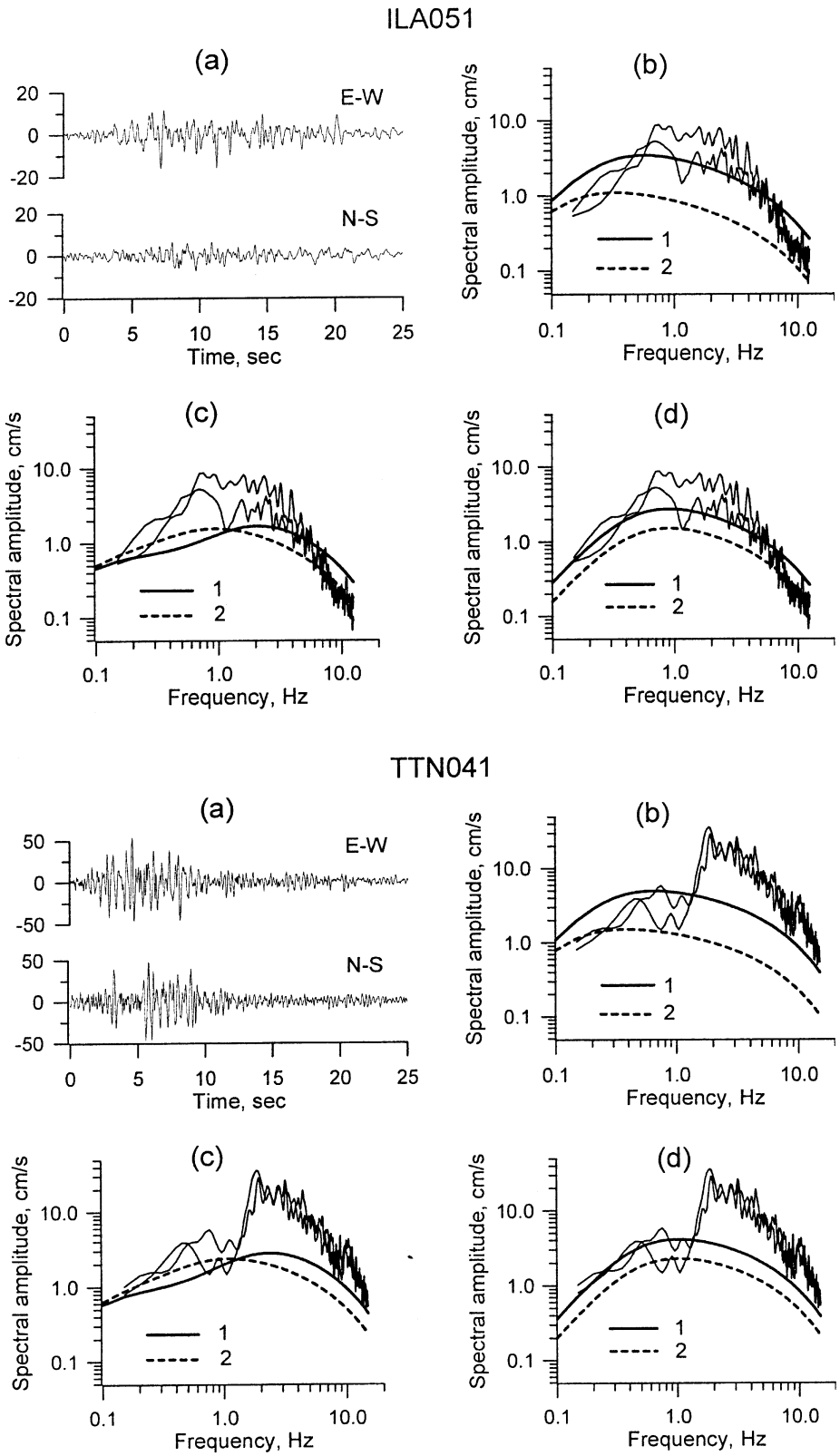

Fig. 5. Aftershock EQ92107, examples of comparison between observed and modelled data. a, Horizontal components of ground acceleration recordings, cm/s^2; b,c,d, comparison between observed Fourier amplitude spectra of ground acceleration (horizontal components, thin lines) and simulated very hard rock spectra (thick lines); b, single-corner-frequency model, $M_0 = 6.0 \times 10^{25}$ dyn cm, $\Delta\sigma = 150$ bars (line 1) and 20 bars (line 2); c, two-corner-frequency models, $M_0 = 6.0 \times 10^{25}$ dyn cm, ENA-model (line 1) and CAL-model (line 2); d, single-corner-frequency model, $M_0 = 1.8 \times 10^{25}$ dyn cm, $\Delta\sigma = 250$ bars (line 1) and $M_0 = 1.0 \times 10^{25}$ dyn cm, $\Delta\sigma = 150$ bars (line 2).

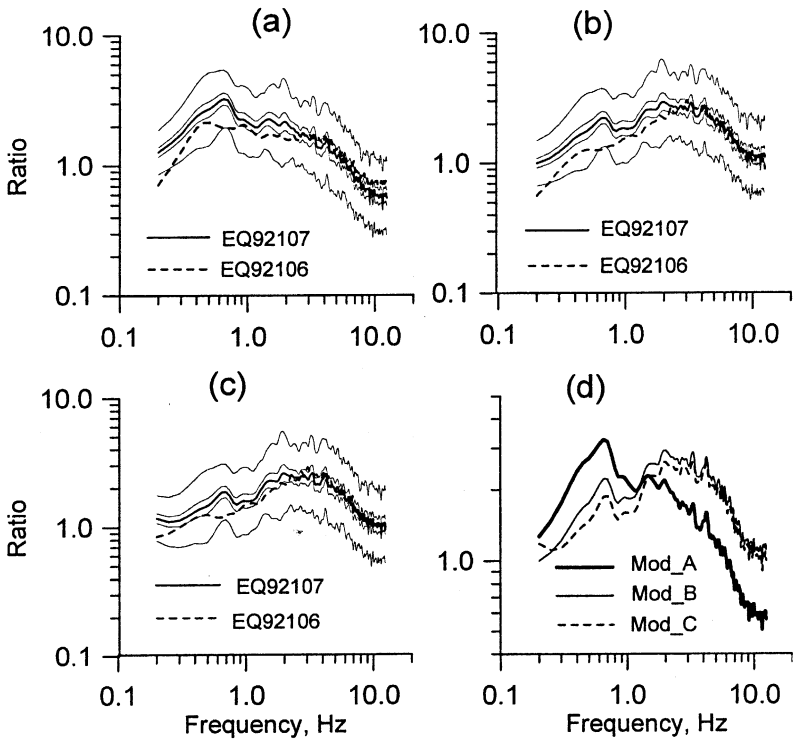

Fig. 6. Aftershock EQ92107. Characteristics of site class B amplification functions (ratio between observed and modelled spectra); thick lines show mean-amplitude values, thin lines denote ± 1 standard deviation of the mean (standard error) and ± 1 standard deviation limits. The correspondent mean-amplitude amplification curves from EQ92106 data are shown in plots (abc) by dashed curves. a, Two-corner-frequency ENA-model of the very hard rock spectra; b, two-corner-frequency CAL-model; c, single-corner-frequency model ($M_0 = 1.4 \times 10^{25}$ dyn cm, $\Delta\sigma = 150$ bars); d, comparison of the mean-amplitude amplification functions evaluated using the considered (plots a, b, c) models.

The seismic moment values reported for the Chi–Chi earthquake vary from 0.5×10^{27} dyn cm [59] to 3.38×10^{27} dyn cm (Harvard CMT Catalogue). Therefore, we also evaluated the spectral ratios for various seismic moment values. Fig. 7 shows comparison between observed acceleration spectra (examples; HWA026, eastern direction; TTN024, southern direction) and theoretical hard rock spectra modelled using the reported value of seismic moment ($M_0 = 3.4 \times 10^{27}$ dyn cm) for the case of single-corner-frequency spectral model and two-corner-frequency models. The Atkinson's model proposed for eastern North America, providing a good agreement with empirical spectra in low frequency part, shows the higher amplitudes at intermediate and high frequencies (Fig. 7c).

Second, we also consider the single-corner-frequency model based on Eqs. (7) and (8) namely: the mean value of M_0 for local magnitude 7.3 is 5.2×10^{25} dyn cm (confidence limits between 8.25×10^{24} and 3.19×10^{26} dyn cm); the maximum value of stress parameter is 315 bars. The mean value of the seismic moment is close to 'short-period seismic moment' value ($0.8–1.6 \times 10^{26}$ dyn cm), that can be evaluated from 'seismic moment–short-period seismic moment" relationship suggested in Refs. [3,54] (see Figs. 2–12 in Ref. [54]. Third, we used the single-frequency model based on parameters suggested in Ref. [55] for the largest asperity of the Chi–Chi mainshock fault model (seismic moment of 1.0×10^{26} dyn cm and stress parameter of 200 bars). It should be noted, that the seismic moment of the largest asperity is almost equal to the 'short-period seismic moment'. In this case (Fig. 7d), there is no significant difference between the modelled spectra, especially for intermediate and high frequencies. Again, to be consistent in the choice of the key parameters, we used the second pair of parameters (asperity) for evaluation of site class B amplification.

Fig. 8 compares the mean-amplitude amplification function evaluated for the mainshock and considered aftershocks (eastern and southern stations) on the basis of accepted two- and single-corner-frequency spectral models. In this case, two values of seismic moment were used, namely: source 1, $M_0 = 3.4 \times 10^{27}$ dyn cm and source 2, $M_0 = 1.0 \times 10^{27}$ dyn cm. Ideally, for the case of linear soil response, the site amplification functions should not depend on earthquake magnitude. Therefore, if the proper hard rock spectral models are accepted for various magnitudes, the characteristics (averaged amplitudes and shape) of ratios between observed and modelled spectra should be approximately the same for different earthquakes. In contrast, with the case of two-corner-frequency ENA-model (Fig. 8a), the mean-amplitude amplification functions evaluated for the mainshock and aftershocks on the basis of chosen single-corner-frequency TWN-model (Fig. 8c) are almost the same both by shape and amplitudes. The two-corner-frequency CAL-model (Fig. 8b, source 1) based on Harvard seismic

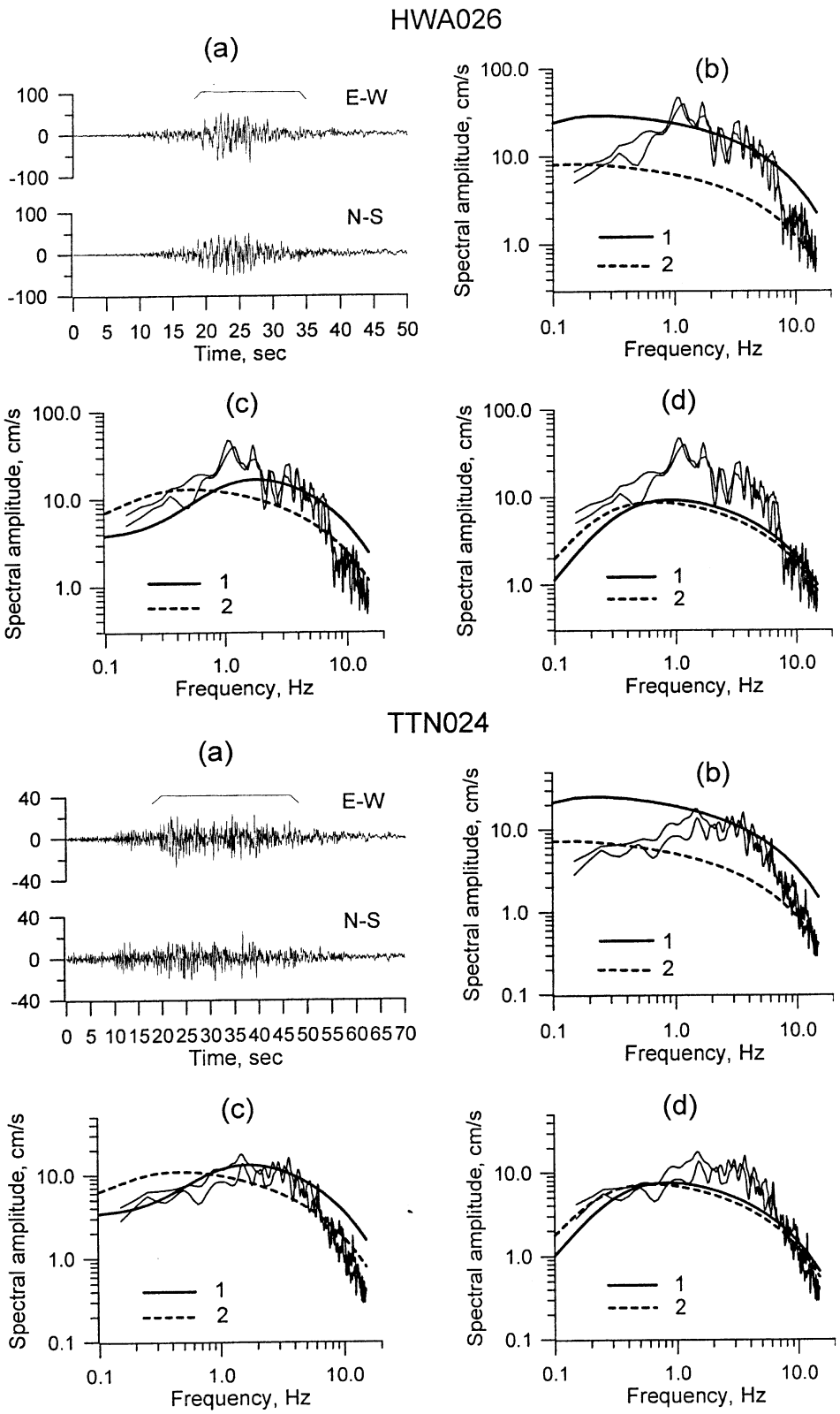

Fig. 7. The Chi–Chi earthquake mainshock, examples of comparison between observed (eastern, station HWA026, and southern, station TTN024, directions from the source) and modelled data. a, Horizontal components of ground acceleration recordings, cm/s^2; b,c,d, comparison between observed Fourier amplitude spectra of ground acceleration (horizontal components, thin lines) and simulated very hard rock spectra (thick lines); b, single-corner-frequency models, $M_0 = 3.4 \times 10^{27}$ dyn cm, $\Delta\sigma = 150$ bars (line 1) and 20 bars (line 2); c, two-corner-frequency models, $M_0 = 3.4 \times 10^{27}$ dyn cm, ENA-model (line 1) and CAL-model (line 2); d, single-corner-frequency model, $M_0 = 5.2 \times 10^{25}$ dyn cm, $\Delta\sigma = 300$ bars (line 1) and $M_0 = 1.0 \times 10^{26}$ dyn cm, $\Delta\sigma = 200$ bars (line 2).

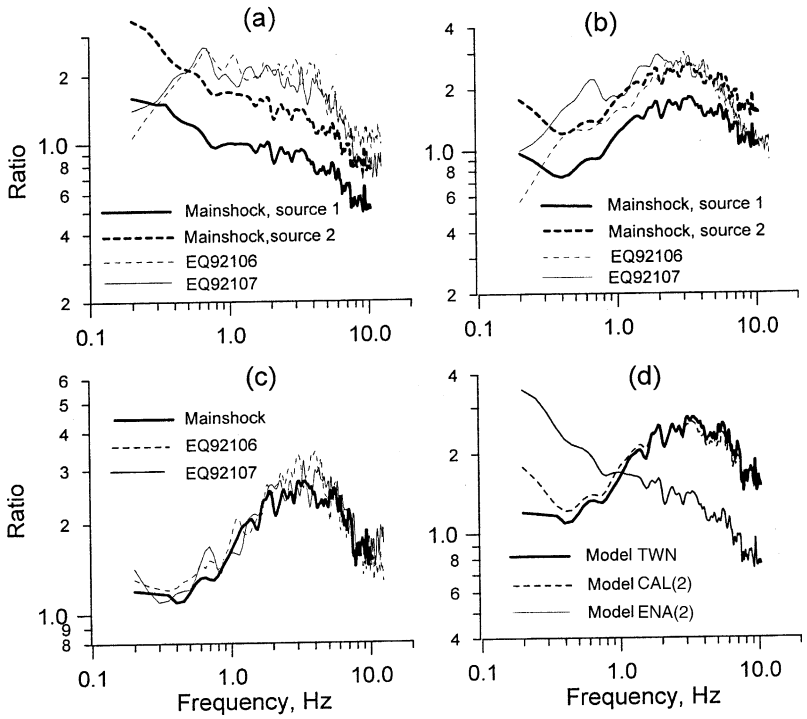

Fig. 8. Comparison of the site class B amplification functions evaluated from the mainshock and considered aftershocks data (stations located to the southern and eastern directions from the mainshock source). a, Two-corner-frequency ENA-model of the very hard rock spectra; b, two-corner-frequency CAL-model; c, single-corner-frequency TWN-model; d, comparison of the mean-amplitude amplification functions evaluated jointly for the mainshock and aftershocks data using the considered (plots a, b, c) models. Two values of seismic moment were used for the case of mainshock and two-corner-frequency models, namely: source 1, $M_0 = 3.4 \times 10^{27}$ dyn cm; source 2, $M_0 = 1.0 \times 10^{27}$ dyn cm.

moment value seems to overestimate hard rock spectra within the entire considered frequency range. The seismic moment value of 1.0×10^{27} dyn cm gave a good agreement (Fig. 8d, source 2) with the amplification determined from aftershocks data. The comparison of mean-amplitude amplification curves, which were evaluated for the case of mainshock using the ENA- and CAL-models and single-corner-frequency (asperity-based) model of hard rock spectra is shown in Fig. 8d.

When analyzing recordings obtained at site class B stations located toward the northern direction from the mainshock source, it is necessary to consider the ground motion enhancing to the North from the source. Furumura et al. [45] on the basis of numerical 2D and 3D simulation concluded that strong diving S-waves, produced by the large shallow asperity of the Chi–Chi earthquake and the large velocity gradient in the crust rigid bedrock, enhance the ground motion to the North from the source at the epicentral distances between 80 and 120 km at frequency range less than 1 Hz. It has been also shown [36] that the spectra of accelerograms recorded to the North from the mainshock source exhibit the higher amplitudes, as compared with the modelled 'average soil' spectra, for frequencies less than 1–2 Hz, and the difference increase with distance. Thus, when calculating hard rock spectra for the northern class B stations, we used additional distance- and frequency-dependent empirical amplification coefficients (Fig. 9) that were determined in Ref. [36] as ratios between observed and modelled average soil spectra. Fig. 10 shows comparison between observed acceleration spectra and modelled hard rock spectra for the northern stations TAP075 and TAP103 chosen as the examples. Spectral ratios (averaged from two horizontal components) between observed and modelled VHR spectra calculated for considered events are also shown in the figure.

The mean-amplitude spectral ratios estimated using asperity-based single-corner-frequency TWN-spectral models for three considered earthquakes are shown in Fig. 11a. Note that the curves are similar both by shapes and amplitudes. The characteristics of site class B amplification obtained using the data from all considered earthquakes are shown in Fig. 11b and c (mean-amplitude, ± 1 standard

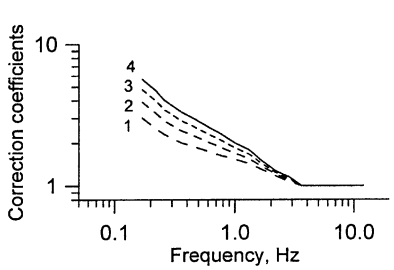

Fig. 9. Empirical frequency- and distance-dependent amplification coefficients for accounting of the peculiarities of seismic waves propagation to the northern direction from the mainshock (see also Ref. [36]). 1: coefficients for distance range 65–75 km; 2: 75–85 km; 3: 85–95 km; 4: 95–105 km.

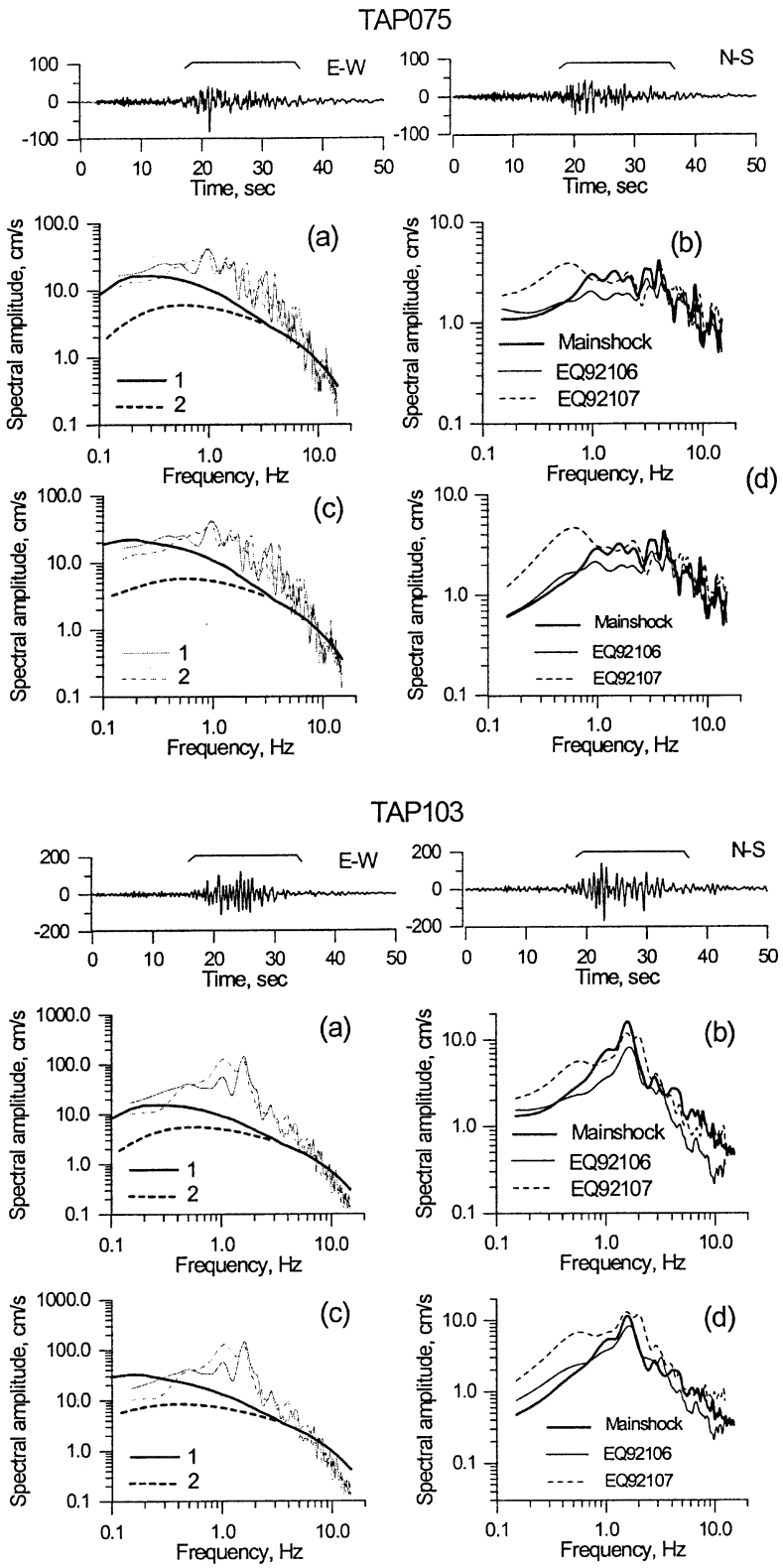

Fig. 10. The Chi–Chi earthquake mainshock, examples of comparison between observed and modelled data (northern direction from the mainshock source). a, Comparison between observed Fourier amplitude spectra of ground acceleration (horizontal components, thin lines) and simulated very hard rock spectra (thick lines), single-corner-frequency model (see text). Modelled spectra are shown for two cases: empirical amplification coefficients were applied (line 1) and were not applied (line 2); b, comparison of the amplification functions (averaged from two horizontal components) obtained for the considered earthquakes using single-corner-frequency model; c, comparison between observed Fourier amplitude spectra of ground acceleration and simulated very hard rock spectra, two-corner-frequency model (see text); d, comparison of the amplification functions obtained for the considered earthquakes using two-corner-frequency model.

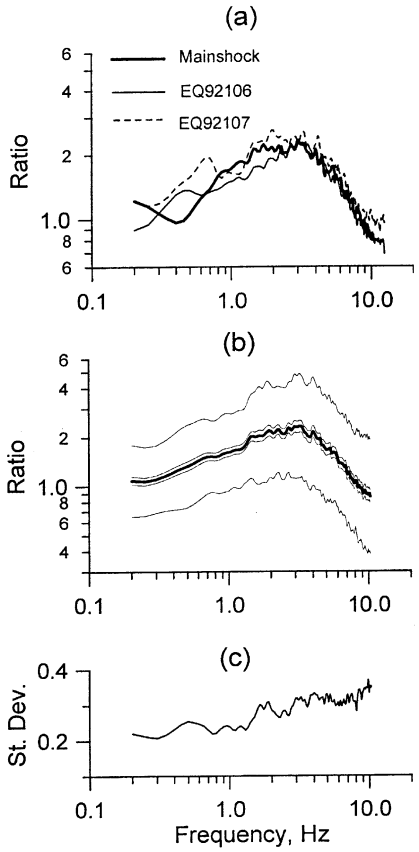

Fig. 11. The site class B amplification functions. a, Comparison of amplification functions (mean-amplitude values) evaluated for the Chi–Chi earthquake mainshock and considered aftershocks; b, characteristics of site class B amplification functions for the Taiwan region evaluated using the whole data set, thick lines show mean-amplitude values, thin lines denote ± 1 standard deviation of the mean (standard error) and ± 1 standard deviation limits; c, distribution of standard deviation of the amplification values versus frequency.

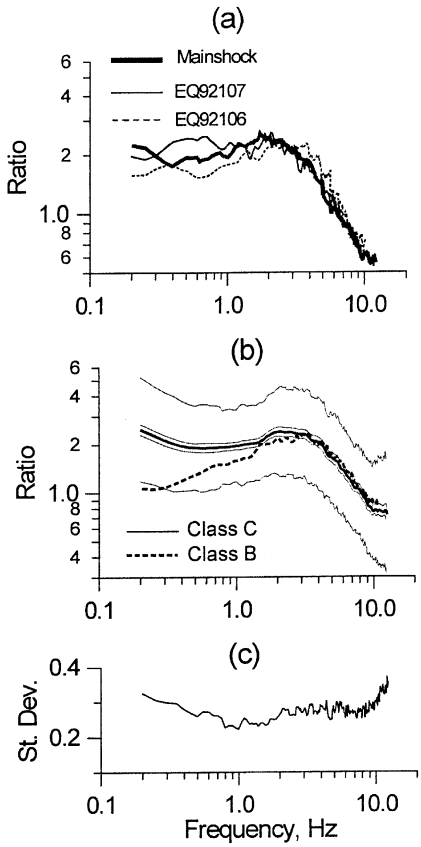

Fig. 12. The site class-C amplification function. a, Comparison of amplification functions (mean-amplitude values) evaluated for the Chi–Chi earthquake mainshock and considered aftershocks; b, characteristics of site class C amplification functions for the Taiwan region evaluated using the whole data set, thick lines show mean-amplitude values, thin lines denote ± 1 standard deviation of the mean (standard error) and ± 1 standard deviation limits, dashed line. Mean-amplitude site class-B amplification is shown by dashed line; c, distribution of standard deviation of the amplification values versus frequency.

error of the mean and ± 1 standard deviation; distribution of standard deviation versus frequency, respectively). The amplitude of mean-amplification reaches a value of 2.3 at frequency about 3.0 Hz. At the same time, the scatter of individual spectral ratios (represented by the standard deviation) is the least at frequencies less than 1 Hz and, for the higher frequencies, it increases with frequency.

4.5. The Chi–Chi earthquake sequence, site class C

Bearing in mind the agreement of the CAL- and asperity-based spectral models, in this section we consider only the second model. Fig. 12a shows comparison of mean-amplitude amplification functions evaluated for class C stations separately for three considered earthquakes. The characteristics of amplification obtained using the data from all considered earthquakes are shown in Fig. 12b and c (mean-amplitude, ± 1 standard error of the mean and ± 1 standard deviation; distribution of standard deviation versus frequency, respectively). Mean-amplitude amplification evaluated for site class B (see Fig. 11b) is also shown for comparison.

5. Discussion

5.1. Site amplification

In Section 4, we analyzed the ability of various ‘hard rock’ spectral models to describe the frequency content of ground motions during the Chi–Chi earthquake sequence (the mainshock and two strong aftershocks). It has been shown that two spectral models provide the similar results when using the models for evaluation of site amplification functions. The first of the spectral models is two-corner-frequency model proposed for California [2]. In this case, the modelled hard rock spectra for aftershocks are based on the values of seismic moment (Table 2) reported in Harvard CMT Catalogue (www.seismology.harvard.edu). The second one is one-corner-frequency TWN-model that is

based on parameters (seismic moment M_0 and stress drop $\Delta\sigma$) of the Chi–Chi mainshock subsources (asperities) proposed in Ref. [55].

Let us consider characteristics of amplification (ratio between the observed and modelled hard rock spectra) for site classes B and C in the Taiwan island. Because the CAL- (two-corner-frequency) and asperity-based (single-corner-frequency) spectral models show the same results, we will further discuss the amplification obtained using the second model (Figs. 11 and 12). It is seen that the curves reflect the general expected relation between class B and class C amplifications—the softer soil would provide amplification at the lower frequencies (see also Ref. [26]).

The distribution of standard deviation versus frequency reflects the influence of the variety of rock properties for sites that are classified as rock (class B) or soft rock or very dense soil (class C) sites. For class B sites (Fig. 11c), the standard deviation values sharply increase up to 0.3–0.32 log unit for frequencies greater than 1 Hz and they are approximately steady for frequencies 3.0–7.0 Hz. For this site condition, the amplification peaks of the spectral ratios lie within frequency range of 2–4 Hz. The amplification functions include the sharp and single peak ones (for example, station TAP103, amplification up to 12 times at frequencies around 1.5 Hz, Fig. 10), the moderate and broad amplification ones (for example, station TAP075, amplification up to 3.0 at frequencies 2–4 Hz, Fig. 10), as well as other types of curves. The standard deviation values increase for frequencies more than 8.0 Hz reflecting the large scatter among particular spectral ratios in the range. Several stations exhibit relatively high spectral amplitudes and even prominent amplification peak (see for example, stations TTN041 and HWA26, Figs. 3 and 5) within this frequency range. In contrast, other stations are characterized by high attenuation of spectral amplitudes with the frequency increase (for example, stations ILA051 and TAP103, Figs. 3 and 10).

The same frequency-dependent behaviour of distribution of standard deviation values is observed for class C sites (Fig. 12c). However, in this case, frequency range of 0.2–1.0 Hz is characterized by increasing of standard deviation with decreasing of frequency. It is seen from Fig. 1b, that several stations classified as C sites are located in the vicinity of deep alluvium plain area (WCP). The long-period waveforms that include significant surface waves appears to be the common ground-motion characteristics in the area [45,46]. Fig. 13 shows comparison of mean-amplitude amplification curves evaluated separately for stations located in the vicinity of the WCP and outside the area. There is a prominent difference in amplitude for frequencies less than 1 Hz. On the other hand, the difference may be explained by influence of predominant geologic and geomorphologic factors [37].

The obtained site amplifications are the function of a source spectral model chosen. Therefore, the analysis of reliability of the amplification values is necessary both for

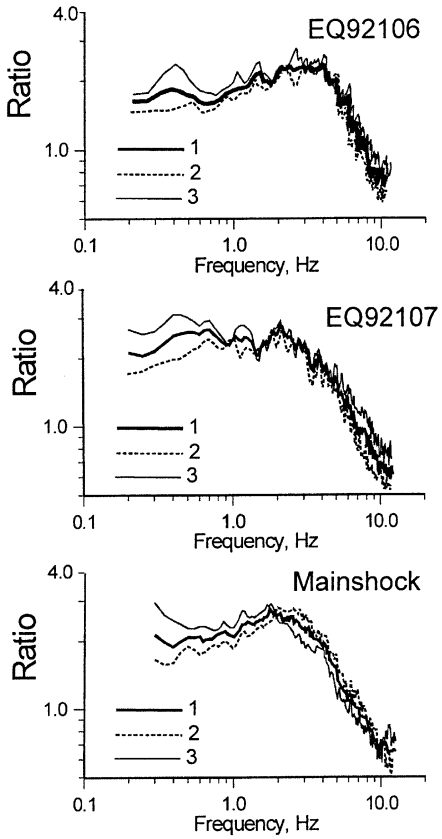

Fig. 13. (1) The site class-C amplification functions evaluated using the whole data set, and (2) separately for records obtained outside the Western Coastal Plain area and (3) in the vicinity of the area.

recognition of ‘true’ site amplification and for judgment of applicability of the used ‘hard rock’ spectral model. The best way of the analysis is a comparison with independent data. However, for the Taiwan region, the amplification functions for generic site classes were obtained only on the basis of response spectra data: response spectral ratios and horizontal-to-vertical ratios (HVSR) of response spectra [37]. The relation between transfer function (ratio of Fourier amplitude spectra) and response spectra is not linear, and we used the following procedure of comparison. First, the amplification functions obtained in this study are compared with the transfer functions proposed for California [26] and Greece [27]. Second, response spectra were calculated using stochastic approach for theoretical VHR site and site classes B and C. The corresponding mean-amplitude amplification functions were used in conjunction with the VHR spectral model for site-dependent ground-motion modelling. Response spectra were calculated for a broad range of magnitudes (5.0–7.5) and distances (20–100 km). The spectral acceleration ratios were evaluated as ratios between the class B and C response spectra and VHR response spectra. The mean-amplitude spectral accelerations ratios (class B/VHR and class C/HR) were compared with mean response spectral ratios calculated in Ref. [37] for the corresponding site classes.

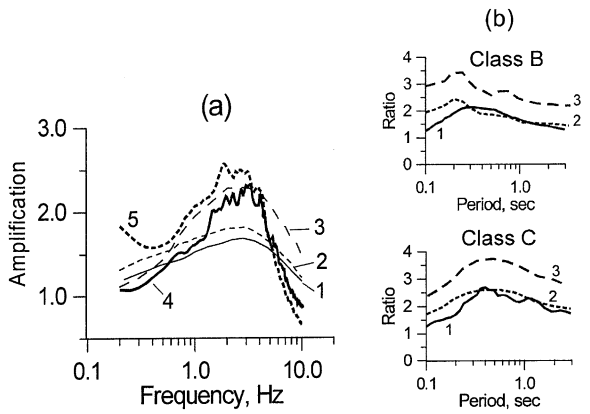

Fig. 14. Comparison of amplification functions evaluated in this study with independent data. a, Generic site amplification (transfer) functions for western America [26] (line 1, soil class B; line 2, soil class C) and Greece [27] (line 3, soil class C); lines 4 and 5, this study, soil class B and C, correspondingly; b, response spectral ratios; 1, mean spectral ratios evaluated in this study, 2, 3, mean and +84 percentile of HVSR obtained in Ref. [37].

Fig. 14a compares mean-amplitude amplifications resulting from the Chi–Chi earthquake data with that proposed for western US [26] and Greece [27]. The Taiwan class C amplification function is shown for the station located outside the WCP area. On the one hand, both classes B and C US amplification functions exhibit lower values than correspondent Taiwan function for frequencies 1–8 Hz. The Hellenic class C amplification, showing in general the same amplitudes as that for Taiwan class C site for frequencies less than 5 Hz, is characterized by the higher amplitudes at high frequencies. Extremely high weathering rate in Taiwan due to the wet climate, which leads to high attenuation of high-frequency radiation, may be considered as the reason of the difference.

Comparison between mean-amplitude spectral acceleration ratios (class B/VHR and class C/VHR), which were evaluated using stochastic approach, and characteristics of empirical response spectral ratios [37] is shown in Fig. 14b. The empirical ratios were evaluated as HVSR of response spectra (see also Refs. [63,64]) calculated from earthquake recordings. The comparison shows that agreement between modelled (B/VHR and C/VHR) and empirical HV spectral ratios is quite good. However, for the case of site class B, the HVSR mean-amplification curve exhibits the higher amplitudes than B/VHR ratios for periods less than 0.2 s. The discrepancy, most probably, is caused by peculiarities of the empirical ground-motion database. The most part of the records, which were used in Ref. [37] were obtained during earthquakes of magnitudes <5.5. To be recorded during small earthquakes, ground-motion acceleration should be characterized by relatively large spectral amplitudes in high-frequency range to produce sufficient amplitudes in the time domain to trigger the instruments. Therefore, the essential part of the acceleration records for small magnitudes may consist on recordings obtained at the sites with high-amplitude and high-frequency site response. When constructing the generalized site amplification functions in this work, we used the all data obtained from the Chi–Chi earthquake mainshock and two aftershocks. The earthquakes were recorded by almost all stations. Unfortunately, in Ref. [37], there is no information what stations had been triggered during the smaller earthquakes.

As far as the amplification curves for classes B and C reveal similar amplitudes and shapes for frequencies larger than 2–3 Hz, there should be, in general, no difference between PGA for these generic site classes. Comparison of distribution of the PGA values versus distance for the considered earthquakes (Fig. 14d) confirms the suggestion. At the same time, the individual observed peak amplitudes show a good agreement with the modelled PGA calculated using the VHR spectral model and mean-amplitude amplification curve (class C). As expected, the VHR model provides a ‘lower limit’ estimations.

5.2. Spectral models

Our goal was to evaluate ability of various spectral models to describe the seismic radiation from large earthquakes. It is necessary to note that we do not consider, in detail, complicated distribution of slip on the Chi–Chi earthquake source. When working with Fourier spectra, the dependence of duration and intensity of ground motions on the azimuth to the observation site is neglected. In the case of future earthquakes, even the gross slip distribution and other rupture characteristics are unknown. It is possible to evaluate only the range of magnitudes and most likely area of the event occurrence. Therefore every kind of simulation for future earthquake would contain significant uncertainty. There is a question: what parameters of future seismic sources should be used for strong ground-motion simulation for the purposes of seismic hazard assessment? We try to obtain the answer by variation of key parameters of the applied models.

The value of seismic moment M_0, which is determined from long-period waves at teleseismic distances, and moment magnitude M_W, which is determined directly from M_0, characterize parameters of the entire source (its dimensions and averaged slip). Large shallow earthquakes, however, are usually multiple shocks. The number and properties of the subsources (heterogeneities) determine short-period radiation [60]. Koyama and Zheng [3] proposed to use so-called ‘short-period seismic moment’ (M_1) for evaluation of short-period source excitation of earthquake. The value of M_1, which is evaluated from Fourier spectra of P-phases from large earthquakes, closely relates to the property of the heterogeneities.

Table 5 lists parameters of the earthquakes (seismic moment and magnitudes) that were reported and used for modelling with comparison of the Koyama-Zheng ‘short-period’ parameters. It is necessary to note that, for the mainshock, the ‘short-period seismic moment’ corresponds

to the Hanks–Kanamori moment magnitude M_W of 6.4–6.8. It has been shown by Tsai and Huang [40], that distribution of the Chi–Chi PGA values versus distances is equivalent to what would be predicted for $M_W = 6.6$, 6.0, and 6.2 from Campbell's, Boore and Joyner's and Sadigh et al.'s attenuation models, respectively (Fig. 15). Thus, following Refs. [3,10,20,60–62] among others, it is possible to conclude that, at least for the case of shallow thrust earthquake, the short-period seismic waves are generated mainly from the fracture of small-scale fault heterogeneities.

At the same time, the results of modelling shows that, at least in the far-fields zone, the use of two-corner-frequency source model of the earthquake spectrum that is based on long-period seismic moment value (M_0) is equivalent to the use of single-corner model that is based on parameters of major subfault. Bearing in mind the above-mentioned comparison of PGA distribution, it is possible to suppose, that large earthquakes in Taiwan generate more intensive low-frequency radiation. These features could be explained, either, by the properties of the Earth's crust in the regions and, or by the rupture characteristics. For example, the ground-motion spectra from earthquakes, which occurred in rigid and consolidated medium (eastern North America, or Central Asia), are characterized by predominance of high-frequency amplitudes [1,6,10]. The phenomenon could be described by the presence of strong asperities or barriers along the fault plane: stronger the asperities, higher the amplitudes of the high-frequency part of the spectra.

the Taiwanese class B and class C mean-amplification curves for frequencies more than 2–3 Hz. Extremely high weathering rate in Taiwan due to the wet climate, which leads to high attenuation of high-frequency radiation, may be considered as the reason of the difference.

It is also necessary to note the prominent influence of geologic and geomorphologic factors, on site amplification function for the considered cases of rock (class B) and soft rock or very dense soil (class C) sites. The influence is reflected by large variations of amplitudes and predominant frequencies between particular stations with the same site class that was assigned on the basis of the rock age and geological classification. Therefore, as it has been noted in Ref. [37], further studies on site classification should be carried out using more specific subsurface geotechnical data.

The results of evaluation of the spectral models, which were obtained in this study, may be considered as a basis for subsequent analyses of peculiarities of the Chi–Chi earthquake strong ground motion in the near-field zone including 'finite-fault' effect and nonlinear soil response. At the same time, it is possible to study the response of sediment-filled basins (for example, the Taipei basin, TAP array) on earthquakes of various magnitudes, distances and location including the Chi–Chi earthquake and aftershocks. On the other hand, the characteristics of generalized amplification functions should be further evaluated, using the available records of other earthquakes. These are the tasks of future research.

Acknowledgements

The authors are grateful to anonymous reviewers for their his comments and suggestions. The study was supported by the National Science Council of the Republic of China under grant NSC89-2811-E-319-0005.

References

[1] Atkinson GM. Earthquake source spectra in Eastern North America. Bull Seismol Soc Am 1993;83:1778–98.
[2] Atkinson GM, Silva W. Stochastic modeling of California ground motions. Bull Seismol Soc Am 2000;90:255–74.
[3] Koyama J, Zheng SH. Excitation of short-period body-waves by great earthquakes. Phys Earth Planet Interiors 1985;37:108–23.
[4] Hanks TC, McGuire RK. The character of high-frequency strong ground motion. Bull Seismol Soc Am 1981;71:2071–95.
[5] Boore DM. Stochastic simulation of high frequency ground motion based on seismological model of the radiated spectra. Bull Seismol Soc Am 1983;3:1865–94.
[6] Boore DM, Atkinston GM. Stochastic prediction of ground motion and spectral response parameters at rock sites in eastern North America. Bull Seismol Soc Am 1987;77:440–67.
[7] Boore DM, Joyner WB. Estimation of ground motion at deep-soil sites in Eastern North America. Bull Seismol Soc Am 1991;81:2167–85.
[8] Atkinson GM, Boore DM. Ground-motion relations for eastern North America. Bull Seismol Soc Am 1995;85:17–30.
[9] Lam N, Wilson J, Hutchinson G. Generation of synthetic earthquake accelerograms using seismological modelling: a review. J Earthquake Engng 2000;4:321–54.
[10] Chernov YK. Strong ground motion and quantitative assessment of seismic hazard. Tashkent: Fan Publishing House; 1989. (in Russian).
[11] Sokolov VY, Chernov YK. On the correlation of seismic intensity with Fourier acceleration spectra. Earthquake spectra 1998;14:679–94.
[12] Sokolov VYu. Seismic intensity and Fourier acceleration spectra: revised relationship. Earthquake Spectra 2002;18:161–87.
[13] Brune JN. Tectonic stress and the spectra of seismic shear waves from earthquakes. J Geophys Res 1970;75:4997–5009.
[14] Beresnev IA. What we can and cannot learn about earthquake sources from the spectra of seismic waves. Bull Seismol Soc Am 2001;91:397–400.
[15] Rovelli A, Bonamassa O, Cocco M, Di Bona M, Mazza S. Scaling laws and spectral parameters of the ground motion in active extensional areas in Italy. Bull Seismol Soc Am 1988;78:550–60.
[16] Hwang LH, Kanamori H. Teleseismic and strong-motion source spectra from two earthquakes in eastern Taiwan. Bull Seismol Soc Am 1989;79:935–44.
[17] Mahdavian A, Sasatani T. Predictive modeling of earthquake ground motion in the northern part of Japan. Proceeding of the Fifth US National Conference on Earthquake Engineering, Chicago, July 10–14, vol. III.; 1994. p. 231–40.
[18] Sokolov VY. Empirical models for estimating Fourier amplitude spectra of ground acceleration in the northern Caucasus (Racha seismogenic zone). Bull Seismol Soc Am 1997;87:1401–12.
[19] Sokolov VY. Spectral parameters of ground motion in different regions: comparison of empirical models. Soil Dyn Earthquake Engng 2000;19:173–81.
[20] Gusev A. Descriptive statistical model of earthquake source radiation and its application to an estimate of short-period strong motion. Geophys J R Astron Soc 1983;74:787–808.
[21] Boatwright J, Choy G. Acceleration source spectra anticipated for large earthquakes in northeastern North America. Bull Seismol Soc Am 1992;82:660–80.
[22] Haddon R. Earthquake source spectra in eastern North America. Bull Seismol Soc Am 1996;86:1300–13.
[23] Atkinson GM, Silva W. An empirical study of earthquake source spectra for California earthquakes. Bull Seismol Soc Am 1997;87:97–113.
[24] Atkinson GM, Boore DM. Evaluation of models for earthquake source spectra in eastern North America. Bull Seismol Soc Am 1998;88:917–34.
[25] Borcherdt R. Estimates of site-dependent response spectra for design (metodology and justification). Earthquake Spectra 1994;10:617–51.
[26] Boore DM, Joyner WB. Site amplification for generic rock sites. Bull Seismol Soc Am 1997;87:327–41.
[27] Klimis NS, Margaris BN, Koliopoulos PK. Site-dependent amplification functions and response spectra in Greece. J Earthquake Engng 1999;3:237–70.
[28] International Conference of Building Officials (ICBO). Uniform Building Code, Whitterm, California; 1997. p. 492.
[29] Building Seismic Safety Council (BSSC). 1997 Edition NEHRP recommended provisions for seismic regulations for new buildings and other structures, FEMA 302/303, Part 1 (Provisions) and Part 2 (Commentary), developed for the Federal Emergency Management Agency, Washington, DC; 1998. p. 337.
[30] Atkinson GM. An alternative to stochastic ground-motion relation for use in seismic hazard analysis in eastern North America. Seismol Res Lett 2001;72:299–306.
[31] Shin TC, Kuo KW, Lee WHK, Teng TL, Tsai YB. A preliminary report on the 1999 Chi–Chi (Taiwan) earthquake. Seismol Res Lett 2000;71:24–30.
[32] Cheng SN, Yeh YT, Loh CH, Chang CH, Shin TC. Strong-motion data reduction for aftershocks of Chi–Chi earthquake. Proceedings of

International Workshop on Annual Commemoration of Chi–Chi Earthquake, September 18–20, NCREE, Taipei, vol. 1.; 2000. p. 275–82.
[33] Shin TC, Teng TL. An overview of the 1999 Chi–Chi, Taiwan, earthquake. Bull Seismol Soc Am 2001;91:895–913.
[34] Sokolov VY, Loh CH, Wen KL. Empirical model for estimating design input ground motions in Taiwan region. Proceedings of International Workshop on Mitigation of Seismic Effects on Transportation Structures, July 12–14, Taipei, Taiwan; 1999. p. 154–63.
[35] Sokolov VY, Loh CH, Wen KL. Empirical model for estimating Fourier amplitude spectra of ground acceleration in Taiwan region. J Earthquake Engng Struct Dyn 2000;29:339–57.
[36] Sokolov VYu, Loh CH, Wen KL. Comparison of the Taiwan Chi–Chi earthquake strong motion data and ground motion assessment based on spectral model from smaller earthquakes in Taiwan. Bull Seismol Soc Am 2002;92:1855–77.
[37] Lee CT, Cheng CT, Liao CW, Tsai YB. Site classification of Taiwan free-field strong-motion stations. Bull Seismol Soc Am 2001;91: 1283–97.
[38] Yagi Y, Kikuchi M. Source rupture process of the Chi–Chi, Taiwan earthquake determined by seismic waves and GPS data. Eos Trans AGU 2000;81:S21A-05.
[39] Earthquake Engineering Research Institute, The Chi–Chi Taiwan earthquake of September 21. EERI special earthquake report; 1999.
[40] Tsai YB, Huang MW. Strong ground motion characteristics of the Chi–Chi, Taiwan earthquake of September 21, 1999. Earthquake Engng Engng Seismol 2002;2:1–21.
[41] Boore DM. Comparison of ground motions from the 1999 Chi–Chi earthquake with empirical predictions largely based on data from California. Bull Seismol Soc Am 2001;91:1212–7.
[42] Boore DM, Joyner WB, Fumal TE. Equations for estimating horizontal response spectra and peak acceleration from western north American earthquakes: a summary of recent work. Seismol Res Lett 1997;68:128–53.
[43] Campbell KW. Empirical near-source attenuation relationships for horizontal and vertical components of peak ground acceleration, peak ground velocity, and pseudo-absolute acceleration response spectra. Seismol Res Lett 1997;68:154–79.
[44] Sadigh K, Chang CY, Egan JA, Makdisi F, Youngs RR. Attenuation relationships for shallow crustal earthquakes based on California strong-motion data. Seismol Res Lett 1997;68:180–9.
[45] Furumura T, Koketsu K, Wen KL, Furumura M. Numerical simulation of strong ground motion during the Chi–Chi, Taiwan, earthquake. Proceedings of International Workshop on Annual Commemoration of Chi–Chi Earthquake, September 18–20, NCREE, Taipei, vol. 1.; 2000. p. 222–32.
[46] Huang CT, Chen SS. Near-field characteristics and engineering implications of the 1999 Chi–Chi earthquake. Earthquake Engng Engng Seismol 2000;2:23–41.
[47] Anderson J, Hough S. A model for the shape of the Fourier amplitude spectrum of acceleration at high frequencies. Bull Seismol Soc Am 1984;74:1969–93.
[48] Li C, Chiu HC. A simple method to estimate the seismic moment from seismograms. Proc Geol Soc China 1989;32:197–207.
[49] Tsai CCP. Relationships of seismic source scaling in the Taiwan region. Terrestial Atmos Ocean Sci 1997;8:49–68.
[50] Sokolov VY, Loh CH, Wen KL. Empirical study of sediment-filled basin response: a case of Taipei city. Earthquake Spectra 2000;16: 681–707.
[51] Sokolov V. Rough estimation of site response using earthquake ground motion records. Proceedings of Second International Symposium on the Effects of Surface Geology on Seismic Motion (ESG 1998), Yokohama, Japan, December 1–3; 1998. p. 517–22.
[52] Sokolov VY, Loh CH, Wen KL. Empirical models for site and region-dependent ground-motion parameters in Taipei area: a unified approach. Earthquake Spectra 2001;17:313–31.
[53] Sokolov VY, Loh CH, Wen KL. Site-dependent input ground motion estimations for the Taipei area: a probabilistic approach. Probab Engng Mech 2001;16:177–91.
[54] Koyama J. The complex faulting process of earthquakes. Dordrecht: Kluwer Academic Publishers; 1997.
[55] Irikura K, Kamae K, Dalguer LA. Source model for simulating ground motion during the 1999 Chi–Chi earthquake. Proceedings of International Workshop on Annual Commemoration of Chi–Chi Earthquake, September 18–20, NCREE, Taipei, Taiwan, vol. 1.; 2000. p. 1–12.
[56] Liu LF, Wen KL. The site response of Lanyang basin on the Chi–Chi earthquake sequence. Proceedings of International Workshop on Annual Commemoration of Chi–Chi earthquake, September 18–20, Taipei, Taiwan, vol. I.; 2000. p. 294–304.
[57] Somerville P. Engineering application of strong ground motion simulation. Tectonophysics 1993;218:195–219.
[58] Fletcher JB. Ground motion in the Taipei and Ilan basin. Seismol Res Lett 2001;2:283.
[59] Lee SJ, Ma KF. Rupture process of the 1999 Chi–Chi, Taiwan, earthquake from the inversion of teleseismic data. Terrestial Atmos Ocean Sci 2000;11:591–608.
[60] Aki K. Strong motion seismology. In: Erdic MO, Toksoz MN, editors. Strong ground motion seismology. Series C: Mathematical and physical sciences; 1987. p. 3–40.
[61] Arefiev SS. Gradation of spectra from near earthquakes. In: Macroseismic and instrumental studies of strong earthquakes, (Problems of engineering seismology, iss. 26), Moscow: Nauka; 1995. (in Russian), p. 134–41.
[62] Somerville P. Magnitude scaling of near fault ground motions. Proceedings of International Workshop on Annual Commemoration of Chi–Chi earthquake, September 18–20, Taipei, Taiwan, vol. I. 2000, p. 59–70.
[63] Yamazaki F, Ansary MA. Horizontal-to-vertical spectrum ratio of earthquake ground motion for site characterization. Earthquake Engng Struct Dyn 1997;26:671–89.
[64] Zare M, Bard PY, Ghafory-Ahtiany M. Site characterization for the Iranian strong motion network. Soil Dyn Earthquake Engng 1999;18: 101–23.